Rotational bands in ^{77}Rb: Spectroscopy near the $Z=38$ deformed shell gap

A. Harder,[1] A. Jungclaus,[1] M. K. Kabadiyski,[1,*] D. Kast,[1] K. P. Lieb,[1] D. Rudolph,[1,†] M. Weiszflog,[1,‡] T. D. Johnson,[1] G. Winter,[2] C. J. Gross,[3] R. A. Cunningham,[4] W. Gelletly,[4,§] J. Simpson,[4] D. D. Warner,[4] I. G. Bearden,[5] T. Shizuma,[5,‖] G. Sletten,[5] D. Foltescu,[6,¶] H. A. Roth,[6] Ö. Skeppstedt,[6] and B. J. Varley[7]

[1]*II. Physikalisches Institut, Universität Göttingen, D-37073 Göttingen, Germany*

[2]*Forschungszentrum Rossendorf, D-01314 Dresden, Germany*

[3]*Physics Division, Oak Ridge National Laboratory, Oak Ridge, Tennessee 37831*

[4]*Daresbury Laboratory, Warrington WA4 4AD, United Kingdom*

[5]*Niels Bohr Institute, DK-4000 Roskilde, Denmark*

[6]*Department of Physics, Chalmers University of Technology, S-412 96 Göteborg, Sweden*

[7]*Schuster Laboratory, University of Manchester, Manchester M13 9PL, United Kingdom*

(Received 13 November 1996)

The γ decays of high spin states in ^{77}Rb populated in the reaction ^{40}Ca(^{40}Ca,3p)^{77}Rb were studied with the EUROGAM I γ-ray spectrometer at Daresbury Laboratory, in conjunction with the recoil mass separator. The data were used to extend or establish three positive parity and five negative parity bands in ^{77}Rb. Level lifetimes and sidefeeding times were then measured with the NORDBALL γ-ray spectrometer, using the Doppler shift attenuation method. A very detailed level scheme including many weakly populated states was established and the bands were observed over large spin ranges. The deduced lifetimes demonstrate the high collectivity of the excited states and are consistent with their having large prolate deformations. The structures of the bands and their crossings are discussed in relation to the large shell gap at prolate deformation $\beta_2 \approx 0.4$. [S0556-2813(97)01104-7]

PACS number(s): 21.10.Re, 23.20.Lv, 25.70.Gh, 27.50.+e

I. INTRODUCTION

In recent years, nuclei near the strongly deformed $N=Z=38$ shell gap at prolate deformation $\beta_2 \approx 0.4$ have been investigated in much detail. These studies have been motivated by the interplay between pairing forces, nuclear shapes, and rotation on the one hand and the interactions between and among $g_{9/2}$ protons and neutrons on the other hand. Studies of high spin states in the nucleus ^{77}Rb ($Z=37$, $N=40$) have been carried out by Lister *et al.* [1] and Lühmann *et al.* [2] using rather simple detector setups which were sufficient to identify the lowest lying bands of both parities and to measure some lifetimes. These studies showed both bands to have large and rather similar deformations of $|\beta_2| \approx 0.4$ and near-rigid shapes as deduced from the equality of the kinematical and dynamical moments of inertia. A suppression of static pairing correlations, due to the pronounced shell gap in the Nilsson scheme at $\beta_2 = +0.4$, is thought to be responsible for this finding [3,4]. Large prolate deformation has also been derived for the $3/2^-$ ground state from resonance laser spectroscopy on a mass-separated ^{77}Rb beam [5]. Very recently we have reported on the properties of the positive parity, yrast, and yrare bands in ^{77}Rb [6] and have again used the argument of suppressed static pairing to interpret the unusual band crossing between the two bands.

The present work was motivated by the wish to extend the bands towards higher spins, i.e., beyond the expected alignments, to identify further bands based on the other Nilsson orbits and, finally, to determine more lifetimes, especially in new bands. We emphasize that ^{77}Rb is among the most strongly deformed nuclei (ground state) in the Chart of Nuclides and many high spin phenomena at large deformation can be readily studied in the strongly populated bands near the ground state. Furthermore, the ^{77}Rb+3p exit channel has the largest part of the cross section of the ^{40}Ca + ^{40}Ca fusion reaction at the applied beam energy of 128 MeV and therefore offers, by using modern large γ-detection arrays [7], very favorable conditions to obtain a rather complete high spin scheme. This paper is organized as follows: Section II contains some details of the two experiments and the data reduction procedure. In Sec. III the experimental results are presented, which are discussed in Sec. IV, in terms of the cranked shell model and compared with rotational structures in neighboring nuclei.

II. EXPERIMENTS AND DATA REDUCTION

A. The EUROGAM I experiment

High spin states in ^{77}Rb were populated via the reaction ^{40}Ca(^{40}Ca,3p) using the 128 MeV ^{40}Ca beam provided by the Daresbury tandem accelerator. The resulting γ radiation was detected with the EUROGAM I array [8,7] which was

*Present address: SAP AG, D-69190 Walldorf, Germany.

†Present address: Sektion Physik, LMU München, D-85748 Garching, Germany.

‡Present address: The Svedberg Laboratoriet, S-75121 Uppsala, Sweden.

§Present address: Physics Department, University of Surrey, Guildford, GU2 5XH, United Kingdom.

‖Present address: University of Tsukuba, Ibaraki 305, Japan.

¶Present address: INFN, Laboratori Nazionali di Legnaro (Padova), Italy.

TABLE I. Summary of the matrices sorted for ^{77}Rb from the EUROGAM I data.

Matrix	Multiplicity	Gate (keV)	Number of events
CaCa	$\gamma\gamma$		1.2×10^9
DCO	$\gamma\gamma$		4.4×10^7
77Rb1 ($\pi=+$)	$\gamma\gamma\gamma$	147, 160, 162, 185, 502, 743, 954	7.6×10^7
77Rb2 ($\pi=-$)	$\gamma\gamma\gamma$	223, 247, 368, 470, 576, 665, 845	7.1×10^6
77Rb3	$\gamma\gamma\gamma$	239, 280, 323, 352, 434, 441, 495	5.1×10^6

coupled to the Daresbury recoil separator [9,10]. EUROGAM I contained 45 Compton-suppressed Ge detectors at 72° (10 detectors), 86° (5), 94° (5), 108° (10), 134° (10), and 158° (5). The target consisted of 250 μg/cm^2 of ^{40}Ca, enriched to 99.965%, which had been evaporated onto a 10 μg/cm^2 carbon foil and covered with a flash of gold to prevent oxidation. It was mounted with the carbon side facing the recoil separator. Radioactive sources of ^{152}Eu, ^{133}Ba, and (for high γ-ray energies) ^{88}Y were used for energy and efficiency calibration of the Ge detectors.

The recoil separator allowed the identification of A and Z of the recoiling nuclei, so recoil-γ coincidence events as well as two- and higher-fold γ coincidences were recorded. With a relative cross section of 54(3)%, ^{77}Rb was the most strongly populated nucleus in the reaction. However, the high line density in the spectra, together with the considerable Doppler broadening resulting from the high velocity of the recoiling nuclei, rendered gating in a conventional $\gamma\gamma$ matrix quite difficult. This was especially true for weak transitions and those at higher γ energies. In order to obtain unambiguous information, $\gamma\gamma\gamma$ and higher-fold coincidence events were used to construct the level scheme. For this purpose, three two-dimensional $\gamma\gamma$ matrices were sorted by imposing the additional condition that the double event was in coincidence with a characteristic third γ transition. The gating conditions for the matrices are summarized in Table I: One matrix (77Rb1) was sorted for the positive parity states in ^{77}Rb and one (77Rb2) for the negative parity states. A third one (77Rb3) was sorted because of the observation of a previously unknown sequence of γ transitions in the ^{77}Rb recoil-γ spectrum at 239, 280, 323, 352, 434, 441, and 495 keV, which turned out to belong to an excited, weakly populated band. To illustrate the quality of the data Fig. 1 shows different types of spectra for this band: In the projection of the conventional $\gamma\gamma$ matrix [displayed in Fig. 1(a)] the above transitions are indistinguishable. In the recoil-γ spectrum [see Fig. 1(d)], which contains ^{77}Rb transitions only, they can be clearly identified [10]. In the $\gamma\gamma\gamma$ matrix 77Rb3 sorted on condition that one of the coincident transitions is of the above-mentioned energies, the labeled transitions are significantly enhanced [cf. Fig. 1(b)] so that gating in this matrix resulted in clean spectra, as demonstrated in Fig. 1(c). The triple-γ events allowed the identification of weakly populated states, to set gates on transitions on top of the bands in order to verify forking band structures and to construct the level scheme.

The geometry of the EUROGAM I setup also allowed the assignment of spins from the angular correlations of the γ rays. For this purpose, a matrix (DCO) was constructed in which γ events recorded at 158° were sorted against those recorded at 86° and 94°. The determined coincidence intensities Y yielded directional correlations of oriented states (DCO ratios), here defined as

$$R_{\mathrm{DCO}} := \frac{Y(\gamma_1 \text{ at } 158^\circ;\ \text{gated with } \gamma_2 \text{ at } 86^\circ,94^\circ)}{Y(\gamma_1 \text{ at } 86^\circ,94^\circ;\ \text{gated with } \gamma_2 \text{ at } 158^\circ)}, \tag{1}$$

with the gate (γ_2) set on an $E2$ transition. The DCO ratios were not corrected for the detection efficiencies of the individual detectors because the relative efficiency of the five detectors in the 158° ring was found to be equal to that of the ten detectors at 86° and 94° within the 3% accuracy of the efficiency calibration. The DCO ratios were evaluated to obtain information about the multipole character of the transi-

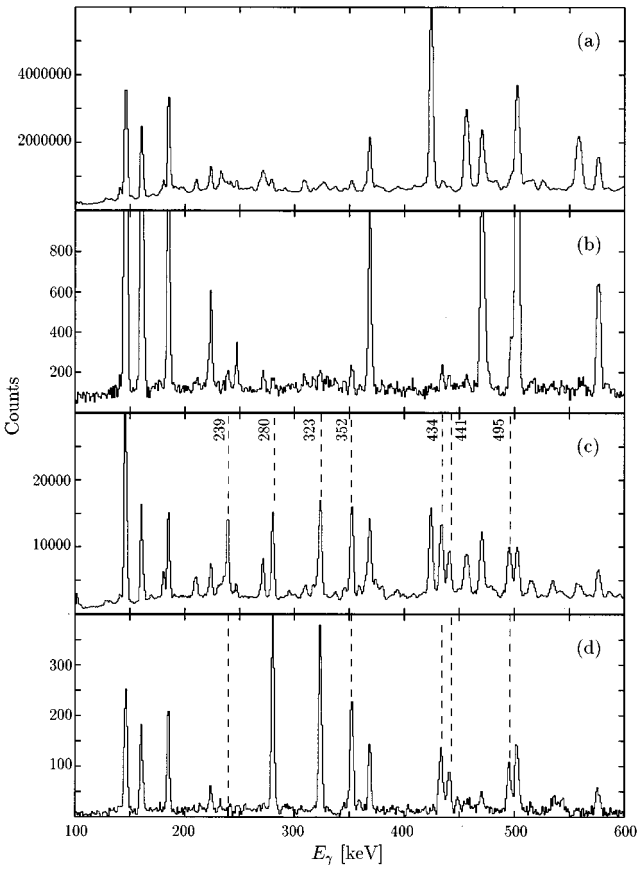

FIG. 1. Coincident γ-ray spectra in ^{77}Rb obtained under different gating conditions. The transitions of band $N5$ are labeled by their energies: (a) total $\gamma\gamma$ projection, (b) recoil-γ projection, (c) projection of the $\gamma\gamma\gamma$ matrix ''77Rb3,'' (d) gate on the 239 keV transition in the $\gamma\gamma\gamma$ matrix ''77Rb3.''

TABLE II. Experimental sidefeeding times in the reaction channel ^{40}Ca(^{40}Ca,3p)^{77}Rb.

E_x (keV)	I^π	E_γ (keV)	τ_{SF}[a] (ps)	τ_{SF}[b] (ps)
6525	$33/2^+$	1519	0.07(1)	
5441	$29/2_2^+$	1112	0.15(3)	
5006	$29/2^+$	1332	0.11(1)	
3674	$25/2^+$	1145	$0.22\binom{4}{2}$	0.38(8)
2630	$19/2^+$	1040	$0.29\binom{30}{16}$	
2529	$21/2^+$	953		0.65(6)
1576	$17/2^+$	743	3.0(5)	
5639	$29/2^-$	1336	0.10(1)	
4303	$25/2^-$	1169	$0.16\binom{3}{1}$	
3134	$21/2^-$	1009	0.35(4)	0.56(10)
2680	$19/2^-$	963	$0.95\binom{45}{25}$	
2125	$17/2^-$	845	1.13(10)	0.93(10)

[a]This work.
[b]Reference [18].

tions. Some 60 DCO ratios were deduced. In some cases, two gates were summed up in order to improve the counting statistics. This procedure does not significantly affect the resulting DCO ratio, as shown in a recent work by Kabadiyski *et al.* [11]. The expected values are $R_{\rm DCO}=1.0$ for stretched $E2$ transitions and $R_{\rm DCO}\approx 0.5$ for stretched pure dipole transitions [11]. $\Delta I=0$ transitions also show values of $R_{\rm DCO}\approx 1$. Thus, in order to distinguish between stretched $E2$ and $\Delta I=0$ transitions, further criteria like parallel transitions or yrast arguments have been taken into account.

B. The experiment at NORDBALL

A Doppler-shift attenuation (DSA) experiment was performed at the Niels-Bohr Institute at Risø, using the same reaction and beam energy. This time the target consisted of a thin ^{40}Ca layer (400 μg/cm^2), evaporated onto a gold foil of 14 mg/cm^2 thickness and covered with a bismuth layer (200 μg/cm^2) to prevent oxidation. This layered target structure stopped all evaporation residues, but allowed the beam ions and the evaporated light particles (p, α, n) to pass through. The γ radiation was detected by means of the NORDBALL array, which contained 19 Compton-suppressed Ge detectors in this experiment. They were positioned at 37° (4 detectors), 79° (5), 101° (5), and 143° (5) with respect to the beam direction. In the backward hemisphere an array of 30 BaF_2 detectors was placed and served as a multiplicity filter. Additionally, particle detectors were used in this particular experiment: evaporated neutrons were registered in seven BC503 scintillators [12] one of which was placed at 0°, a second one at 37°, and the remaining five at 63°. Protons and α particles were detected in a 4π silicon ball [13] surrounding the target. All the (triples) events containing at least two coincident Ge signals and one BaF_2 signal, or one Ge signal, one neutron scintillator signal and one BaF_2 signal were written on tape. A ^{152}Eu source was used to calibrate the γ-ray detectors.

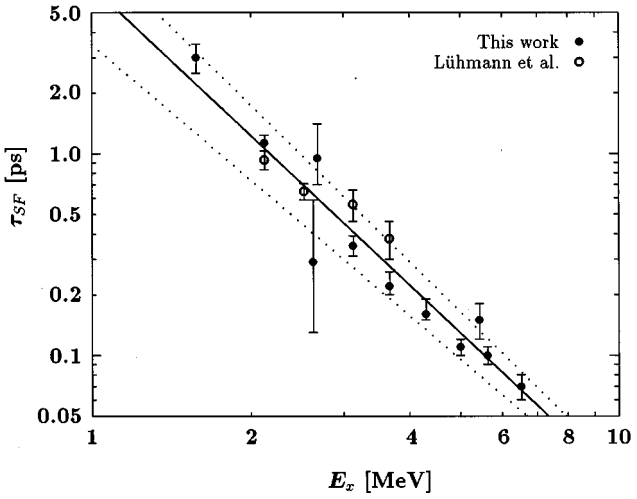

FIG. 2. Correlation between the sidefeeding time $\tau_{\rm SF}$ and the level energy E_x. The open circles indicate the values from the work of Lühmann [18].

Two asymmetric matrices were sorted for the data analysis. The first matrix contained all $\gamma\gamma$ coincidence events with at least one γ ray registered at 143°, the second matrix required at least one Ge signal at 37°. Furthermore, separate spectra were generated for each reaction channel by selecting light evaporated particles. In the case of ^{77}Rb, the registration of three protons was demanded in coincidence with the observed γ event. Contaminations from other reaction channels (e.g., from the $4p$ channel ^{76}Kr) could be removed by successively subtracting the respective isotopic spectra from each other. Such ''clean'' isotopic spectra were sorted for two different observation angles in order to obtain additional information on the γ-ray multipolarity. As the angular correlations are symmetric with respect to 90°, the events registered in the Ge detectors at 37° and 143° were combined, as well as those at 79° and 101°. Stretched $E2$ and $\Delta I=0$ transitions are expected to show a larger intensity at 37°/143° than at 79°/101°, whereas stretched $\Delta I=1$ transitions show the opposite behaviour. Thus, the ratio

$$r_Y=\frac{Y_\gamma(37°)+Y_\gamma(143°)}{Y_\gamma(79°)+Y_\gamma(101°)}, \tag{2}$$

of the γ-ray intensities in the clean particle-γ projections supplies further information on the multipolarity of the respective transition: stretched $E2$ transitions and $\Delta I=0$ transitions resulted in a ratio of $r_Y=1.1(1)$ as opposed to $\Delta I=1$ transitions which have $r_Y=0.5(1)$. These values allowed a cross check on the DCO ratios and yielded additional information on weaker transitions, whose DCO ratios could not be evaluated in the EUROGAM I experiment.

Lifetimes were obtained by evaluating the Doppler-broadened line shapes in the 37° and 143° coincidence spectra. The observed line shapes were compared with calculated line shapes based on the Monte Carlo code DOPPIDIF which simulates the time-dependent velocity distribution of the recoiling nuclei [14,15]. In these simulations, reactions occur-

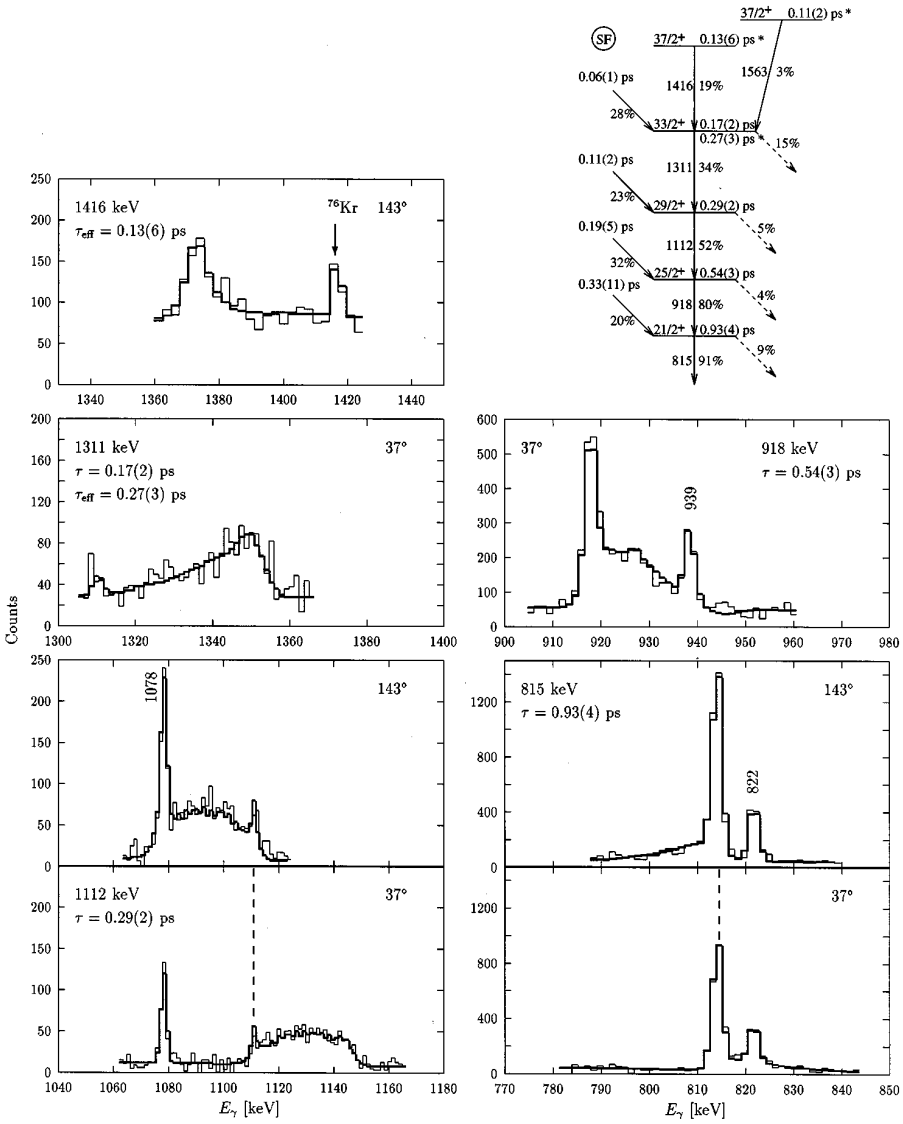

FIG. 3. Doppler broadened line shapes of transitions in the bands $P1/P3$ observed at 143° and 37° to the beam direction. Overlapping, nonbroadened contaminant lines were also included in the fit. The inset illustrates the feeding pattern used.

ring at different depths in the target, the kinematics of the particle evaporation process as well as the slowing down and straggling of the recoiling nuclei were taken into account. The calculation of the velocity distribution was based on the electronic and the nuclear stopping power functions according to Lindhard *et al.* [16]. Furthermore, cascade feeding from higher lying levels and continuum side feeding were taken into account.

Cristancho and Lieb [17] have performed Monte Carlo simulations for the sidefeeding times in the $A \approx 80$ nuclei. While in a number of nuclei the experimental values were reproduced quite accurately, discrepancies were observed in the case of the reaction ^{40}Ca(^{40}Ca,3p) ^{77}Rb, where Lühmann [18] had already determined a few sidefeeding times. The experimental values differed from the calculated ones by one order of magnitude. Thus, we have tried to check the previous experimental sidefeeding times and to determine additional ones in the present study. For this purpose, excited states with ''simple'' feeding scenarios were used, i.e., states which — except for the sidefeeding — are populated by just one transition from a discrete state with a known (effective) lifetime. In this case, apart from the intensity ratio, two free parameters govern the decay function when fitting the calculated line shape to the experimental one. The average sidefeeding time τ_{SF} and the lifetime τ of the studied state are correlated with different χ^2 values obtained in the variation of the two parameters; τ_{SF} and τ were optimized by searching for the minimal χ^2 value. Once τ and τ_{SF} were known for a state, this method of analysis was also applied to the state(s) below. A total of 11 sidefeeding times was determined which are summarized in Table II. As expected, a distinct decrease of the sidefeeding times occurs for increasing excitation energy E_x, starting from some picoseconds below 2 MeV down to less than 0.1 ps above 5 MeV excitation energy. As shown in Fig. 2, the relation between τ_{SF} and E_x can be parametrized by

$$\ln\tau_{SF}[\text{ps}] = 0.78(2) - 2.4(1)\ln E_x[\text{keV}]. \quad (3)$$

The previous experimental sidefeeding times [18] are fairly consistent with this finding. The adopted, rather long sidefeeding times again exceed the theoretical values obtained from the previous Monte Carlo simulation of the time evolution of the total γ-decay flux [17].

The further evaluation of the DSA lifetimes in ^{77}Rb was based on the above relation between τ_{SF} and E_x. If possible,

TABLE III. Excitation energies, transition energies, DCO and r_Y ratios, and spin assignments.

E_x (keV)	E_γ (keV)	$Y_{\rm rel}$ at 64°	$R_{\rm DCO}^{(1)}$	Gate[a]	r_Y	Multi-polarity	I_i^π ($\hbar$)	I_f^π ($\hbar$)
			Band $P1$					
146.5(2)	146.5(2)	26.0(58)[b]			0.60(3)	$E1$	$5/2^+$	$3/2^-$
331.1(2)	184.5(2)	35.1(11)[b]	0.79(1)	A	1.10(5)	$E2$	$9/2^+$	$5/2^+$
	24.4[c]					$E2/M1$	$9/2^+$	$7/2^+$
833.1(2)	502.0(2)	100.0(34)	0.79(1)	B	1.11(5)	$E2$	$13/2^+$	$9/2^+$
1575.6(3)	742.6(2)	89.1(27)	0.87(1)	C	1.03(4)	$E2$	$17/2^+$	$13/2^+$
2529.0(3)	953.4(2)	70.6(21)	0.98(2)	B		$E2$	$21/2^+$	$17/2^+$
3674.0(4)	1145.2(2)	52.7(22)	1.04(2)	B		$E2$	$25/2^+$	$21/2^+$
5005.8(4)	1331.7(2)	41.6(18)	0.94(2)	B		$E2$	$29/2^+$	$25/2^+$
6525.1(4)	1519.4(2)	26.1(8)	0.97(3)	B		$E2$	$33/2^+$	$29/2^+$
8316.3(4)	1563(1)	0.7(1)				$E2$	$37/2_2^+$	$33/2_2^+$
	1791.3(2)	6.2(3)	1.05(6)	B		$E2$	$37/2_2^+$	$33/2^+$
10 209.2(5)	1892.8(3)	4.0(2)	0.90(10)	B		$E2$	$41/2_2^+$	$37/2_2^+$
	2041(1)	1.4(1)				$E2$	$41/2_2^+$	$37/2^+$
12 265(1)	2055(1)	0.6(1)				$(E2)$	$(45/2_2^+)$	$41/2_2^+$
	2448(2)	0.4(1)				$(E2)$	$(45/2_2^+)$	$41/2^+$
12558(1)	2349(1)	0.7(1)						$41/2_2^+$
7506(3)	2500(3)	1.4(3)						$29/2^+$
			Band $P2$					
306.7(2)	159.9(5)	20.8(9)[b]			0.88(4)	$E2/M1$[d]	$7/2^+$	$5/2^+$
	162.0(5)	4.2(2)[b]			0.60(3)	$E1$	$7/2^+$	$5/2^-$
803.9(2)	472.9(2)	11.1(4)	0.80(3)	D		$E2/M1$[d]	$11/2^+$	$9/2^+$
	497.2(3)	11.3(4)	0.84(3)	D	0.95(4)	$E2$	$11/2^+$	$7/2^+$
1590.0(2)	757.0(2)	5.0(2)	0.47(8)	E	0.63(3)	$E2/M1$	$15/2^+$	$13/2^+$
	786.1(2)	15.8(5)	0.84(5)	E	0.96(5)	$E2$	$15/2^+$	$11/2^+$
2630.2(3)	1054.6(2)	3.7(4)				$E2/M1$	$19/2^+$	$17/2^+$
	1040.2(2)	15.6(5)	0.96(5)	D		$E2$	$19/2^+$	$15/2^+$
3894.2(3)	220.8(3)	0.2(1)			0.64(4)	$E2/M1$	$23/2^+$	$25/2^+$
	1264.0(2)	15.8(5)	0.95(5)	A		$E2$	$23/2^+$	$19/2^+$
	1364.7(3)	3.3(2)				$E2/M1$	$23/2^+$	$21/2^+$
5345(1)	1451.3(5)	10.1(6)	0.77(6)	E		$E2$	$27/2^+$	$23/2^+$
	1669(1)	1.0(1)				$E2/M1$	$27/2^+$	$25/2^+$
6927(1)	1582.1(5)	5.6(4)	0.72(7)	E		$E2$	$31/2^+$	$27/2^+$
8627(2)	1700(1)	2.0(5)				$(E2)$	$(35/2^+)$	$31/2^+$
			Band $P3$					
1153.3(2)	350.4(7)	0.4(1)			0.47(8)	$E2/M1$	$9/2_2^+$	$11/2^+$
	822.3(3)	3.8(1)	0.80(5)	G	1.01(9)	$\Delta I=0$	$9/2_2^+$	$9/2^+$
	847.0(4)	0.8(2)				$E2/M1$	$9/2_2^+$	$7/2^+$
	1006(1)	0.3(1)				$E2$	$9/2_2^+$	$5/2^+$
1882.2(2)	729.0(2)	4.9(3)	0.93(5)	G	1.28(8)	$E2$	$13/2_2^+$	$9/2_2^+$
	938.5(2)	3.7(2)	0.58(4)	H		$E1$	$13/2_2^+$	$11/2^-$
	1049.0(2)	7.8(9)	0.86(5)	F	1.16(9)	$\Delta I=0$	$13/2_2^+$	$13/2^+$
	1078.1(2)	4.4(5)			0.82(5)	$E2/M1$	$13/2_2^+$	$11/2^+$
2596.4(2)	714.1(2)	19.2(6)	0.99(2)	G	1.09(5)	$E2$	$17/2_2^+$	$13/2_2^+$
	879.4(3)	3.0(2)	0.52(4)	G		$E1$	$17/2_2^+$	$15/2^-$
	1006.9(6)	3.7(4)	0.36(4)	D		$E2/M1$	$17/2_2^+$	$15/2^+$
	1020.9(2)	4.6(3)			1.11(8)	$\Delta I=0$	$17/2_2^+$	$17/2^+$
	1762(1)	0.6(2)				$E2$	$17/2_2^+$	$13/2^+$
3410.9(3)	814.5(2)	24.6(9)	0.96(3)	F	0.94(4)	$E2$	$21/2_2^+$	$17/2_2^+$
	881.9(4)	1.2(4)				$\Delta I=0$	$21/2_2^+$	$21/2^+$
	1838(2)	1.1(1)				$E2$	$21/2_2^+$	$17/2^+$
4329.3(3)	918.4(2)	21.6(21)	0.95(3)	F		$E2$	$25/2_2^+$	$21/2_2^+$
	1801(2)	1.0(1)				$E2$	$25/2_2^+$	$21/2^+$

TABLE III. *(Continued).*

E_x (keV)	E_γ (keV)	Y_{rel} at 64°	$R^{(1)}_{DCO}$	Gate[a]	r_Y	Multi-polarity	I^π_i ($\hbar$)	I^π_f ($\hbar$)
5440.9(4)	1111.6(2)	14.0(6)	0.85(4)	*G*		*E*2	$29/2^+_2$	$25/2^+_2$
	1766.9(5)	1.3(2)				*E*2	$29/2^+_2$	$25/2^+$
6751.8(4)	1311.0(2)	9.2(6)	0.92(5)	*G*		*E*2	$33/2^+_2$	$29/2^+_2$
	1745.8(4)	4.0(4)	0.81(17)	*C*		*E*2	$33/2^+_2$	$29/2^+$
8167.9(5)	1416.1(3)	5.1(2)	1.08(9)	*G*		*E*2	$37/2^+$	$33/2^+_2$
	1643(1)	9.1(16)	0.94(4) [e]	*B*		*E*2	$37/2^+$	$33/2^+$
9817(1)	1649(1)	7.7(9)	0.94(4) [e]	*B*		*E*2	$41/2^+$	$37/2^+$
11 582(2)	1765(1)	5.6(2)	1.03(14)	*C*		*E*2	$45/2^+$	$41/2^+$
13 551(2)	1969(1)	1.4(1)				(*E*2)	$(49/2^+)$	$45/2^+$
15 797(2)	2246(2)	0.9(1)				(*E*2)	$(53/2^+)$	$(49/2^+)$
18 376(2)	2579(3)	0.2(1)				(*E*2)	$(57/2^+)$	$(53/2^+)$
			Band *N*1					
368.0(2)	223.2(2)	8.4(4)	0.57(1)	*H*	0.35(2)	*E*2/*M*1	$7/2^-$	$5/2^-$
	368.2(2)	39.9(12)	0.80(1)	*H*	1.11(5)	*E*2	$7/2^-$	$3/2^-$
943.7(2)	329.3(3)	2.0(1)	$\ll 1$	*I*	0.31(2)	*E*2/*M*1	$11/2^-$	$9/2^-$
	575.7(2)	45.8(14)	0.85(1)	*I*	1.13(5)	*E*2	$11/2^-$	$7/2^-$
	611.9(5)	1.1(2)				*E*1	$11/2^-$	$9/2^+$
1717.0(2)	773.4(2)	36.9(19)	1.03(2)	*H*	1.12(5)	*E*2	$15/2^-$	$11/2^-$
	884.0(3)	Dublett				*E*1	$15/2^-$	$13/2^+$
2680.0(2)	963.1(2)	31.0(16)	1.01(2)	*H*		*E*2	$19/2^-$	$15/2^-$
3823.1(4)	1142.9(2)	26.8(14)	1.04(2)	*H*		*E*2	$23/2^-$	$19/2^-$
5176.1(5)	1055(1)	1.3(2)				*E*2	$27/2^-_2$	$23/2^-_2$
	1352.5(5)	7.6(4)	1.04(6)	*H*		*E*2	$27/2^-_2$	$23/2^-$
6642.1(6)	1465.9(5)	4.7(2)	1.17(10)	*H*		*E*2	$31/2^-_3$	$27/2^-_2$
	1539(1)	1.5(1)				*E*2	$31/2^-_3$	$27/2^-$
8300(1)	1658(1)	2.2(1)	1.35(21)	*H*		(*E*2)	$(35/2^-_3)$	$31/2^-_3$
10 103(1)	1803(2)	1.4(1)				(*E*2)	$(39/2^-_2)$	$(35/2^-_3)$
			Band *N*2					
3229.5(5)	1104.9(4)	4.6(2)	0.58(5)	*J*		*E*2/*M*1	$19/2^-_2$	$17/2^-$
4122.6(6)	893.4(7)	2.7(2)				*E*2	$23/2^-_2$	$19/2^-_2$
5103.5(4)	980(1)	1.9(3)				*E*2	$27/2^-_2$	$23/2^-_2$
	1280.5(2)	13.8(7)	1.06(4)	*H*		*E*2	$27/2^-_2$	$23/2^-$
6299.1(5)	1123.0(2)	3.4(2)	0.88(5)	*H*,*I*		*E*2	$31/2^-$	$27/2^-_2$
	1195.6(2)	10.7(6)	1.15(5)	*H*		*E*2	$31/2^-$	$27/2^-$
7634.6(6)	1335.5(4)	7.8(7)	0.96(6)	*H*		*E*2	$35/2^-$	$31/2^-$
9145.6(10)	1511(1)	6.7(4)	1.00(6)	*H*		*E*2	$39/2^-$	$35/2^-$
10 860(2)	1714(1)	2.6(1)	0.90(9)	*H*,*I*		*E*2	$43/2^-$	$39/2^-$
12 807(2)	1947(1)	1.2(1)				(*E*2)	$(47/2^-)$	$43/2^-$
15 013(3)	2206(2)	0.6(1)				(*E*2)	$(51/2^-)$	$(47/2^-)$
17 485(4)	2472(3)	0.2(1)				(*E*2)	$(55/2^-)$	$(51/2^-)$
			Band *N*3					
144.8(2)	144.7(2)	39.8(59)[b]	0.49(1)	*K*	0.37(2)	*E*2/*M*1	$5/2^-$	$3/2^-$
614.6(2)	246.7(2)	4.4(2)	0.39(2)	*K*	0.31(2)	*E*2/*M*1	$9/2^-$	$7/2^-$
	307.8(2)	1.9(1)			0.69(5)	*E*1	$9/2^-$	$7/2^+$
	470.0(2)	57.8(17)	0.82(1)	*K*	1.14(4)	*E*2	$9/2^-$	$5/2^-$
1280.2(2)	336.6(2)	1.8(1)	0.35(4)	*H*	0.26(2)	*E*2/*M*1	$13/2^-$	$11/2^-$
	476.4(5)	1.1(1)			0.68(4)	*E*1	$13/2^-$	$11/2^+$
	665.4(2)	57.6(18)	0.88(1)	*J*	1.10(5)	*E*2	$13/2^-$	$9/2^-$
2124.7(3)	407.6(3)	0.9(1)			0.47(6)	*E*2/*M*1	$17/2^-$	$15/2^-$
	534.7(5)	1.0(1)				*E*1	$17/2^-$	$15/2^+$
	844.5(2)	50.1(15)	1.00(2)	*K*		*E*2	$17/2^-$	$13/2^-$
3133.8(3)	1009.1(2)	40.6(21)	1.06(3)	*K*		*E*2	$21/2^-$	$17/2^-$

TABLE III. *(Continued).*

E_x (keV)	E_γ (keV)	$Y_{\rm rel}$ at 64°	$R^{(1)}_{\rm DCO}$	Gate[a]	r_Y	Multi-polarity	I^π_i ($\hbar$)	I^π_f ($\hbar$)
4303.2(4)	1169.4(2)	27.6(14)	0.98(3)	J		$E2$	$25/2^-$	$21/2^-$
5638.8(5)	1335.6(2)	21.8(12)	0.94(4)	J		$E2$	$29/2^-$	$25/2^-$
7198(1)	1559(1)	6.5(3)	0.80(7)	J		$(E2)$	$(33/2^-_2)$	$29/2^-$
8892(2)	1694(1)	3.9(2)	0.92(16)	J		$E2$	$(37/2^-_3)$	$(33/2^-_2)$
10 774(3)	1882(2)	1.7(3)				$(E2)$	$(41/2^-_3)$	$(37/2^-_3)$
8832(2)	1634(1)	2.3(3)				$(E2)$	$(37/2^-_2)$	$(33/2^-_2)$
10 365(2)	1533(1)	1.6(3)				$(E2)$	$(41/2^-_2)$	$(37/2^-_2)$
				Band $N4$				
7086.8(6)	1448.0(4)	10.2(5)	0.98(6)	K		$E2$	$33/2^-$	$29/2^-$
8519.5(8)	1432.7(5)	7.1(4)	0.84(7)	J		$E2$	$37/2^-$	$33/2^-$
10 097(2)	1577(1)	5.4(3)	0.76(9)	J		$(E2)$	$(41/2^-)$	$37/2^-$
11 870(2)	1773(1)	2.7(3)	0.99(21)	J		$E2$	$(45/2^-)$	$(41/2^-)$
13 888(3)	2018(2)	1.4(3)				$(E2)$	$(49/2^-)$	$(45/2^-)$
				Band $N5$				
2149.1(4)	1205(2)					$E2/M1$	$11/2^-_2$	$11/2^-$
	1316.1(5)	2.5(2)				$E1$	$11/2^-_2$	$13/2^+$
	1346(1)	1.3(3)				$E2/M1$	$11/2^-_2$	$11/2^+$
	1817.9(5)	0.8(1)				$E1$	$11/2^-_2$	$9/2^+$
2387.7(4)	238.6(2)	1.7(2)			0.48(3)	$E2/M1$	$13/2^-_2$	$11/2^-_2$
	1107.5(5)	0.9(4)				$E2/M1$	$13/2^-_2$	$13/2^-$
2667.7(4)	280.0(2)	2.0(3)			0.41(3)	$E2/M1$	$15/2^-_2$	$13/2^-_2$
	518(1)	<1				$E2$	$15/2^-_2$	$11/2^-_2$
	1092.1(5)	0.5(1)				$E1$	$15/2^-_2$	$17/2^+$
2991.0(4)	323.3(2)	2.3(2)			0.42(3)	$E2/M1$	$17/2^-_2$	$15/2^-_2$
	603(1)	0.8(3)				$E2$	$17/2^-_2$	$13/2^-_2$
	866(1)	0.6(2)				$\Delta I=0$	$17/2^-_2$	$17/2^-$
3342.7(4)	351.7(2)	2.4(3)			0.44(3)	$E2/M1$	$19/2^-_3$	$17/2^-_2$
	675.2(5)	1.9(2)			1.00(10)	$E2$	$19/2^-_3$	$15/2^-_2$
	813.7(5)	0.2(1)				$E1$	$19/2^-_3$	$21/2^+$
3775.8(5)	433.4(3)	2.4(3)			0.37(2)	$E2/M1$	$21/2^-_3$	$19/2^-_3$
	784.4(5)	1.9(2)				$E2$	$21/2^-_3$	$17/2^-_2$
	1651(1)	2.1(3)				$E2$	$21/2^-_3$	$17/2^-$
4216.3(5)	440.6(2)	1.7(2)			0.33(3)	$E2/M1$	$23/2^-_3$	$21/2^-_3$
	515.4(5)	0.9(1)				$E2/M1$	$23/2^-_3$	$21/2^-_2$
	873.2(5)	2.2(3)				$E2$	$23/2^-_3$	$19/2^-_3$
4758.3(7)	542(1)	0.6(2)				$(E2/M1)$	$(25/2^-_3)$	$23/2^-_3$
	982(1)	1.7(4)				$(E2)$	$(25/2^-_3)$	$21/2^-_3$
	1058(1)	1.1(1)				$(E2)$	$(25/2^-_3)$	$21/2^-_2$
5317.3(8)	606(1)	1.0(3)				$(E2/M1)$	$(27/2^-_3)$	$(25/2^-_3)$
	1101(1)	2.2(5)				$(E2)$	$(27/2^-_3)$	$23/2^-_3$
5956(1)	1198(1)	2.3(4)				$(E2)$	$(29/2^-_3)$	$(25/2^-_3)$
	1244(2)	0.5(2)				$(E2)$	$(29/2^-_3)$	$25/2^-_2$
6615(1)	1298(1)	1.3(3)				$(E2)$	$(31/2^-_2)$	$(27/2^-_3)$
7358(2)	1402(1)	1.4(4)				$(E2)$	$(33/2^-_3)$	$(29/2^-_3)$
8079(2)	1464(2)	0.8(2)				$(E2)$	$(35/2^-_2)$	$(31/2^-_2)$
8954(3)	1596(2)	0.5(2)				$(E2)$	$(37/2^-_4)$	$(33/2^-_3)$
3700.9(6)	1021(1)	2.6(3)	0.38(4)	H,I,L		$\Delta I=1$	$21/2^-_2$	$19/2^-$
4711.2(5)	494.9(2)	1.4(3)			$\ll 1$	$E2/M1$	$25/2^-_2$	$23/2^-_3$
	935.4(5)	1.4(3)				$E2$	$25/2^-_2$	$21/2^-_3$
5851.2(9)	534(1)	0.7(1)				$(E2/M1)$	$(29/2^-_2)$	$(27/2^-_3)$
	1140(1)	0.8(2)				$(E2)$	$(29/2^-_2)$	$25/2^-_2$

TABLE III. *(Continued).*

E_x (keV)	E_γ (keV)	Y_{rel} at 64°	$R_{DCO}^{(1)}$	Gate[a]	r_Y	Multi-polarity	I_i^π ($\hbar$)	I_f^π ($\hbar$)
				Band *X*				
2390.3(5)	1557(1)	1.9(5)						$13/2^+$
3353.4(9)	963(1)	2.2(2)						
	1777(1)	2.2(2)						$17/2^+$
4417.2(9)	1063(1)	1.9(9)						
	1889(1)	0.8(4)						$21/2^+$
5478(1)	1061(1)	1.2(2)						
	1804(2)	< 0.5						$25/2^+$
5681(1)	1264(1)	0.9(2)						
	2007(2)	<1						$25/2^+$
6806(1)	1125(1)	0.6(1)						
1328(1)	0.4(1)							
8263(2)	1457(1)	1.0(2)						
9793(2)	1530(2)	0.4(1)						
11 475(3)	1682(2)	0.2(1)						

[a]*A*, 502 keV; *B*, 743 keV; *C*, 953 keV; *D*, 786 keV; *E*, 1040 keV; *F*, 714 keV; *G*, 815 keV; *H*, 576 keV; *I*, 773 keV; *J*, 845 keV; *K*, 665 keV; *L*, 368 keV.
[b]Intensities are underestimated due to the long lifetimes of the decaying state. See text for details.
[c]Energy calculated from level energy difference.
[d]Multipolarity taken from the angular distribution measurement in [18] [$\delta(E2/M1) = 0.40(10)$].
[e]A common DCO ratio was determined for the doublet 1643/1649 keV.

the two line shapes observed at forward (37°) and backward (143°) angles were evaluated simultanously, thus minimizing the risk of systematic errors due to contaminating lines. As an example, the line shape fits in the newly established positive parity band *P*3 (cf. Sec. III) are shown in Fig. 3. This figure also illustrates the applied feeding pattern, which becomes more and more complex the lower the studied state is situated in the level scheme. Thus, the influence of the experimental errors of the various lifetimes becomes more and more important. In order to study this influence we varied the sidefeeding times and state lifetimes of the populating transitions within their statistical errors in a Monte Carlo way (500 parameter sets) and then performed line shape fits using these 500 different sets of parameters. Figure 4 displays the resulting distribution of the determined lifetimes for the example of the 3411 keV $21/2^+$ state. The distributions of the lifetime values were fitted by Gaussian distribu-

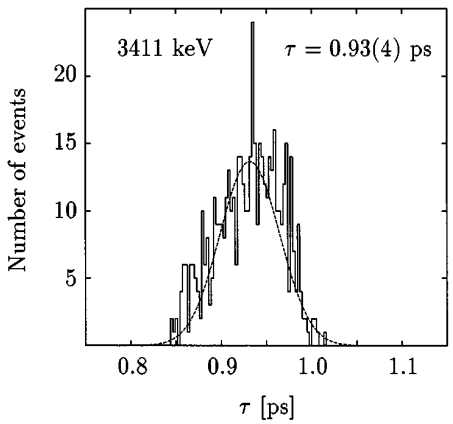

FIG. 4. Monte Carlo distribution of the level lifetimes of the 3411 keV state obtained when statistically varying all the feeding lifetimes within their errors and in each case minimizing χ^2.

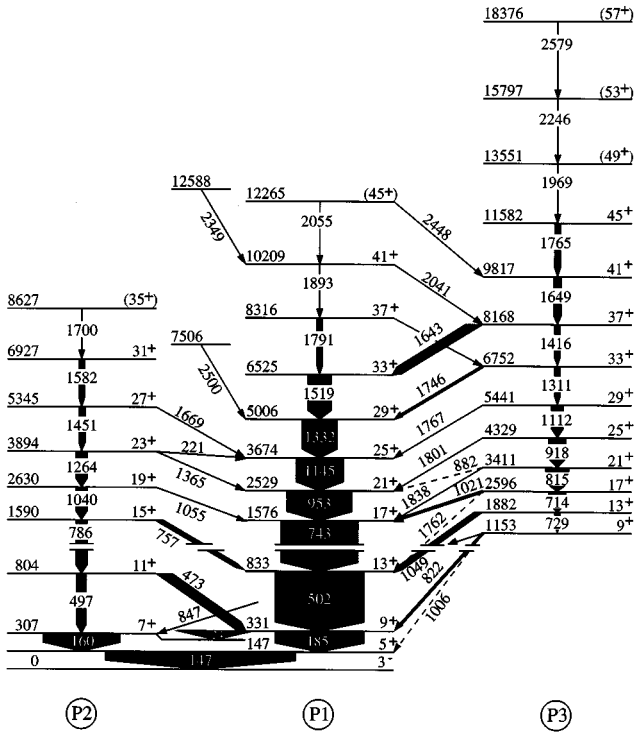

FIG. 5. Positive-parity bands *P*1, *P*2, and *P*3 in ^{77}Rb with their main in-band and interband transitions. Note that the energy axis has been expanded for the states below 1 MeV. Spins are given in units of $\hbar/2$.

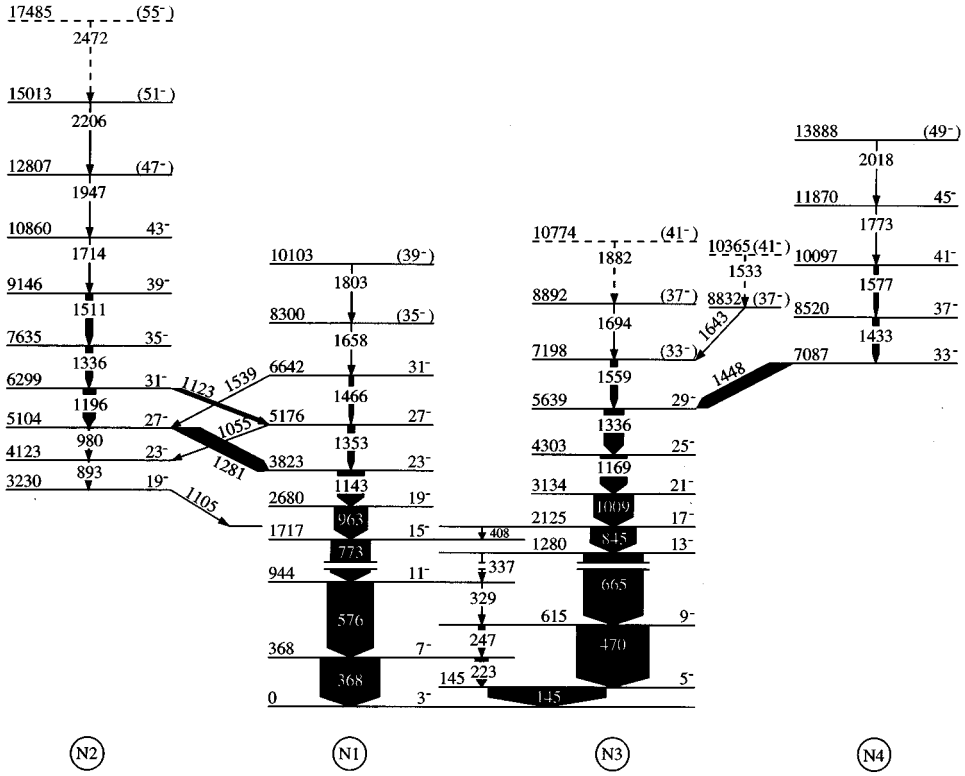

FIG. 6. Same as Fig. 5, but for the negative parity bands $N1-N4$. Several $E1$ transitions connecting the positive and negative parity bands have not been included, but are listed in Table III.

tions, and their centers and FWHM were adopted as lifetime values and errors. The influence of the intensity errors of the populating transitions was much weaker than that of the feeding times and was neglected in this procedure.

III. EXPERIMENTAL RESULTS

The resulting γ-ray energies and intensities, DCO and intensity ratios, level energies and deduced or proposed spin-parity assignments in ^{77}Rb are summarized in Table III, classified according to the main band structures found. All the definite spin assignments are based on the DCO ratios R_{DCO} or intensity ratios r_y [see Eqs. (1) and (2)], while the tentative spin assignments given in brackets follow from the linear increase of the γ-ray transition energy with the spin, typical of near-rigid rotation. In ^{77}Rb this approximation is, indeed, a very good one, as will be discussed further in Sec. IV.

In the previous high spin studies of ^{77}Rb by Lister *et al.* [1] and by Lühmann *et al.* [2], one favored (signature $\alpha=+1/2$) and one unfavored ($\alpha=-1/2$) positive parity band had been identified, extending up to $E_x = 8.2$ MeV and probable spin 37/2. Furthermore, negative parity $\alpha=\pm 1/2$ ground bands up to $E_x = 7.1$ MeV and tentative spin 33/2 had been established. The positive parity high spin states observed in the present work are summarized in Fig. 5. Not only has the favored band $P1$ been extended up to $(45/2^+)$ and the unfavored band $P2$ up to $(35/2^+)$, but a new band $P3$ has been established, which has spins identical with those of the favored band $P1$ and extends up to $E_x = 18\,376$ keV and $I^\pi=(57/2^+)$. Band $P3$ becomes yrast around 7 MeV excitation energy and, therefore, could be followed to a much higher spin value than $P1$ and $P2$. In contrast to most high spin schemes measured in previous studies for this and neighboring nuclei, the second band $P3$ was also seen *below* the crossing point and, indeed, was established down to its presumed $9/2^+$ bandhead. This is a consequence of the large cross section in the $3p$ exit channel and the high efficiency

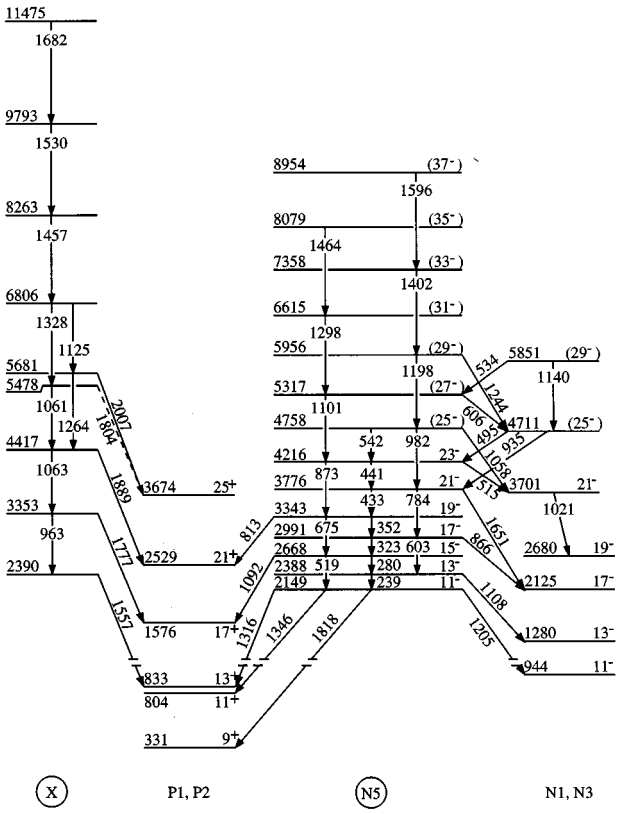

FIG. 7. Same as Fig. 5, but for the bands $N5$ and X.

TABLE IV. Lifetimes and adopted sidefeeding times in ^{77}Rb.

E_x (keV)	I ($\hbar$)	E_γ (keV)	τ_{SF} [a] (ps)	τ_{eff} [b] (ps)	τ_{DSA} [b] (ps)	τ_{DSA} [c] (ps)	τ_{RDDS} [c] (ps)	$\overline{\tau}$ [d] (ps)
*P*1								
10 209	$41/2_2^+$	1893		0.08(3)				$\leqslant 0.11$ [e]
8316	$37/2_2^+$	1791	0.04(1)	0.11(2)	0.06(2)			0.06(2)
6525	$33/2^+$	1519	0.07(2)	0.14(1)	0.04(1)			0.04(1)
5006	$29/2^+$	1332	0.13(3)	0.22(1)	0.07(1)	0.19(4) [e]		0.07(1)
3674	$25/2^+$	1145	0.28(9)		0.15(2)	0.09(4)		0.14(2)
2529	$21/2^+$	953	0.70(26)		0.37(2)	0.32(6)		0.37(2)
1576	$17/2^+$	743	2.23(98)		0.92(4)	1.12(21)	1.27(26)	0.93(6)
833	$13/2^+$	502					9.2(6)	9.2(6)
331	$9/2^+$	185					991(36)	991(36)
147	$5/2^+$	147					7.4(5) ns	7.4(5) ns
*P*2								
5345	$27/2^+$	1451		0.27(3)				$\leqslant 0.30$ [e]
3894	$23/2^+$	1264	0.24(7)	0.39(2)	0.10(2)			0.10(2)
2630	$19/2^+$	1040	0.63(23)		0.19(3)		1.0(5) [e]	0.19(3)
1590	$15/2^+$	786	2.18(95)		0.90(5)	0.88(35)		0.90(5)
804	$11/2^+$	497					5.2(10)	5.2(10)
307	$7/2^+$	160					568(39)	568(39)
*P*3								
8168	$37/2^+$	1416		0.13(6)				$\leqslant 0.19$ [e]
6752	$33/2_2^+$	1311	0.06(1)	0.27(3)	0.17(2)			0.17(2)
5441	$29/2_2^+$	1112	0.11(2)		0.29(2)			0.29(2)
4329	$25/2_2^+$	918	0.19(5)		0.54(3)			0.54(3)
3411	$21/2_2^+$	815	0.33(11)		0.93(4)			0.93(4)
*N*1/*N*2								
6299	$31/2^-$	1196		0.30(5)				$\leqslant 0.35$ [e]
5104	$27/2^-$	1281	0.12(3)		0.21(2)			0.21(2)
3823	$23/2^-$	1143	0.25(8)		0.17(3)			0.17(3)
2680	$19/2^-$	963	0.60(22)		0.35(3)	0.21(8)		0.33(5)
1717	$15/2^-$	773	1.80(77)		0.65(3)	0.97(20)		0.66(5)
944	$11/2^-$	576					4.2(4)	4.2(4)
368	$7/2^-$	368					42(3)	42(3)
*N*3/*N*4								
5639	$29/2^-$	1336		0.23(1)				$\leqslant 0.24$ [e]
4303	$25/2^-$	1169	0.19(5)		0.16(1)	0.20(4) [e]		0.16(1)
3134	$21/2^-$	1009	0.41(14)		0.26(3)	0.17(5)		0.24(3)
2125	$17/2^-$	845	1.07(42)		0.45(4)	0.48(6)		0.46(3)
1280	$13/2^-$	665	3.7(17)		1.29(9)	2.03(25)	1.58(37)	1.39(23)
615	$9/2^-$	470					11.6(8)	11.6(8)
145	$5/2^-$	145					782(39)	782(39)

[a] From Eq. (3).
[b] This work.
[c] Reference [2].
[d] Adopted value.
[e] Effective lifetime.

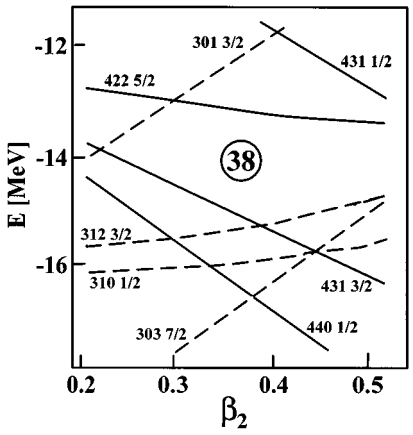

FIG. 8. Nilsson scheme near the $N=Z=38$ deformed shell gap.

of the Ge arrays used. Within all the bands strong stretched $E2$ transitions typical of rotational-aligned structures are observed. We would also like to emphasize that $P1$ and $P3$ are mainly connected by stretched $E2$ transitions, at least above spin $17/2^+$. The bands $P2$ and $P1$, on the other hand, are preferentially connected by $\Delta I=1$ transitions.

Five rotational bands of negative parity have been seen in the present work; they are displayed in Figs. 6 and 7. The arguments concerning the spin assignments for the positive parity states are also valid for most of these states. The bands $N1$, $N2$, $N3$, and $N4$ shown in Fig. 6 appear to be of a decoupled nature and feature long series of stretched $E2$ transitions. Both bands fork into (and communicate with) bands of equal spins: $N2$ and $N1$ around 3 MeV excitation and spin $19/2^-$, and $N3$ and $N4$ around 6 MeV excitation and spin $33/2^-$. Again, the crossing bands $N2$ and $N4$ become yrast above the respective crossing points and, therefore, were followed to somewhat higher energies and spins than the ground bands $N1$ and $N3$: $N2$ was tentatively

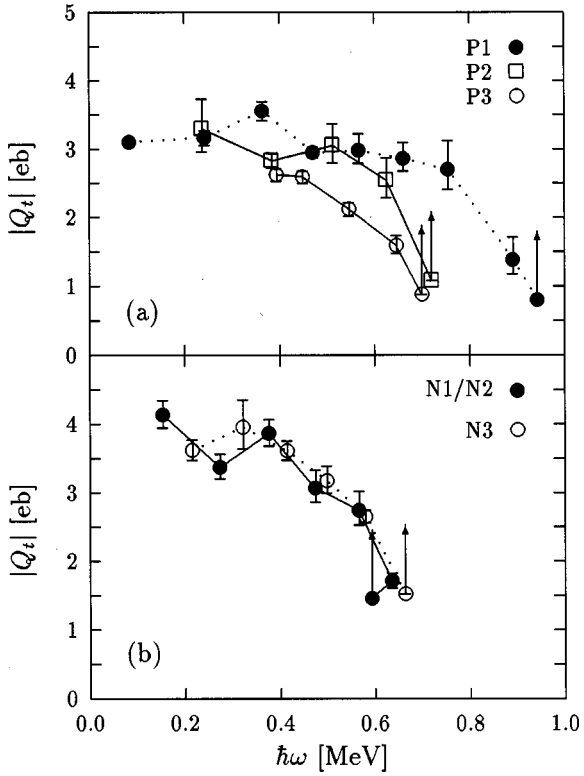

FIG. 9. Summary of the measured transitional quadrupole moments.

established up to $E_x = 17\,485$ keV, $I^\pi=(55/2^-)$ and $N4$ up to $E_x = 13\,888$ keV and $I^\pi=(49/2^-)$. These four bands carry the main γ-ray flux to the 145 keV $5/2^-$ state and the $3/2^-$ ground state.

In contrast, the negative parity band $N5$, identified in this work (see Fig. 7) has very different properties. It is very weakly populated, has a strongly coupled structure with

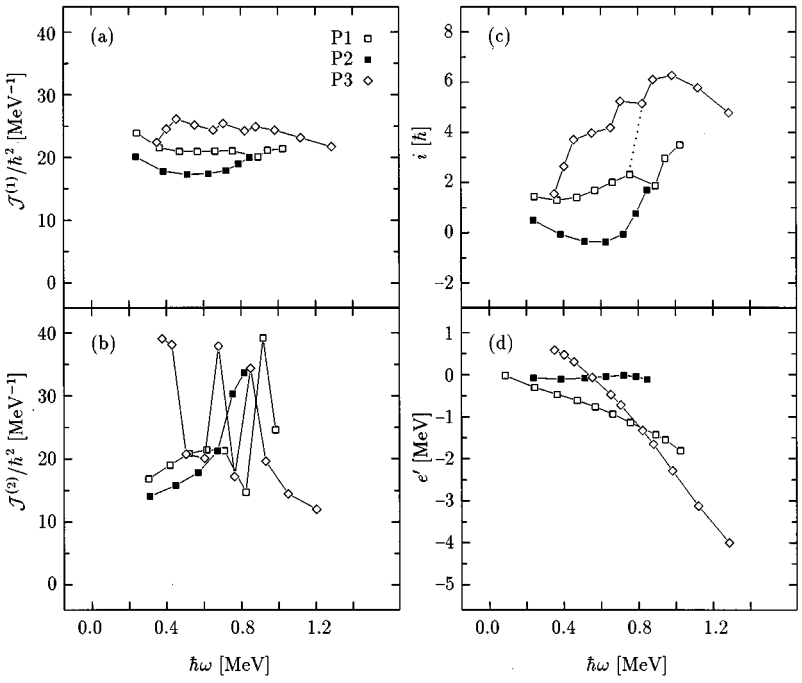

FIG. 10. Kinematical and dynamical moments of inertia $\mathcal{J}^{(1)}/\hbar^2$ and $\mathcal{J}^{(2)}/\hbar^2$, aligned single particle spins i and Routhians e' of the bands $P1$–$P3$.

TABLE V. Reduced transition probabilities $B(E2)$, transitional quadrupole moments Q_t and deformation parameters β_2 in ^{77}Rb.

E_x (keV)	I^π	E_γ (keV)	b	$B(E2)$ (e^2 fm^4)	$\lvert Q_t\rvert$ (e b)	$\lvert\beta_2\rvert$
$P1$						
10 209	$41/2_2^+$	1893	0.74(2)	> 226	> 0.80	> 0.11
8316	$37/2_2^+$	1791	0.90(2)	$660\binom{350}{180}$	$1.38\binom{33}{20}$	0.18(4)
6525	$33/2^+$	1519	1.0	$2500\binom{800}{500}$	$2.70\binom{42}{29}$	0.33(5)
5006	$29/2^+$	1332	1.0	$2800\binom{450}{350}$	$2.86\binom{23}{18}$	0.35(2)
3674	$25/2^+$	1145	1.0	$2950\binom{500}{400}$	$2.98\binom{24}{19}$	0.36(3)
2529	$21/2^+$	953	1.0	2800(150)	2.95(8)	0.36(1)
1576	$17/2^+$	743	1.0	3900(300)	3.55(14)	0.42(1)
833	$13/2^+$	502	1.0	2800(200)	3.16(11)	0.38(1)
331	$9/2^+$	185	< 1	< 3800	< 4.22	< 0.49
$P2$						
5345	$27/2^+$	1451	0.92(2)	> 390	> 1.08	> 0.14
3894	$23/2^+$	1264	0.84(2)	$2100\binom{600}{400}$	$2.54\binom{33}{25}$	0.31(4)
2630	$19/2^+$	1040	0.83(2)	$2950\binom{650}{450}$	$3.05\binom{31}{25}$	0.37(3)
1590	$15/2^+$	786	0.78(1)	2350(150)	2.83(10)	0.34(1)
804	$11/2^+$	497	0.53(2)	$2750\binom{800}{500}$	$3.29\binom{44}{33}$	0.39(5)
$P3$						
8168	$37/2^+$	1416	0.36(5)	> 270	> 0.88	> 0.12
6752	$33/2_2^+$	1311	0.70(3)	$850\binom{150}{100}$	$1.59\binom{14}{12}$	0.20(2)
5441	$29/2_2^+$	1112	0.92(2)	1500(150)	2.12(10)	0.26(1)
4329	$25/2_2^+$	918	0.96(1)	2200(150)	2.59(9)	0.32(1)
3411	$21/2_2^+$	815	0.91(2)	2200(150)	2.62(9)	0.32(1)
$N1/N2$						
6299	$31/2^-$	1196	0.76(2)	> 720	> 1.46	> 0.19
5104	$27/2^-$	1281	0.88(2)	1000(100)	1.72(11)	0.22(1)
3823	$23/2^-$	1143	1.0	$2450\binom{550}{400}$	$2.74\binom{28}{21}$	0.33(3)
2680	$19/2^-$	963	1.0	$3000\binom{550}{400}$	$3.07\binom{26}{21}$	0.37(3)
1717	$15/2^-$	773	0.98(2)	$4400\binom{450}{400}$	$3.86\binom{20}{18}$	0.45(2)
944	$11/2^-$	576	0.94(1)	$2900\binom{350}{300}$	$3.37\binom{19}{17}$	0.40(2)
368	$7/2^-$	368	0.84(2)	$2400\binom{250}{200}$	$4.13\binom{21}{19}$	0.45(2)
$N3/N4$						
5639	$29/2^-$	1336	1.0	> 800	> 1.53	> 0.20
4303	$25/2^-$	1169	1.0	2350(150)	2.65(9)	0.32(1)
3134	$21/2^-$	1009	1.0	$3250\binom{450}{350}$	$3.17\binom{22}{18}$	0.38(2)

TABLE V. *(Continued).*

E_x (keV)	I^π	E_γ (keV)	b	$B(E2)$ (e^2 fm^4)	$\lvert Q_t\rvert$ (e b)	$\lvert\beta_2\rvert$
2125	$17/2^-$	845	0.97(1)	4000(300)	3.61(14)	0.43(2)
1280	$13/2^-$	666	0.96(1)	$4350\binom{900}{650}$	$3.95\binom{40}{31}$	0.46(4)
615	$9/2^-$	470	0.91(1)	$2800\binom{250}{200}$	3.62(15)	0.43(2)

$\Delta I=1$ level ordering (see Fig. 1), and a rather high spin of $K^\pi = 11/2^-$ for its bandhead. In-band transitions as well as a large number of interband transitions to $P1$, $P2$, $N1$, and $N3$ are indicated in Fig. 7. Due to the weak flux in this band, no DCO ratios could be extracted, which led to only tentative spin assignments for the states above 4.5 MeV excitation energy. The spins of the lower members rely on the parallel stretched dipole-quadrupole branches, the definite spin-parity assignments of the states fed by the out-of-band transitions, and the very regular $I(I+1)$ pattern of the level energies. The assigned spin and parity of the 2149 keV bandhead, $I^\pi=11/2^-$, is suggested by its decays to the 944 keV $11/2^-$, 331 keV $9/2^+$, and 804 keV $11/2^+$ states. Another transition which provides unique spin-parity assignments in this band is the 1651 keV $21/2^- \rightarrow 17/2^-$ transition.

A series of seven transitions with energies regularly increasing with spin along the band ''*X*'' (also shown in Fig. 7), connects the 2390 keV state with that at 11 475 keV. The lowest four states of this structure feed the band $P1$ in the spin range $13/2^+ - 25/2^+$ which suggests that they have similar spin values and positive parity. As the lowest transition (963 keV) in this band collects only 2.2% intensity of the 502 keV, $13/2^+ \rightarrow 9/2^+$ transition, no DCO ratios could be measured.

Table IV summarizes the information on the level lifetimes gained in the previous [2,18] and present work. The sidefeeding times included have been taken from the parametrization mentioned in Sec. II B, assuming that they only depend on the excitation energy and not on spin or parity. In general, the DSA level lifetimes deduced in both studies are in fair agreement and do not show systematic deviations from each other. Of course, the much higher counting statistics accumulated in the present experiment and the more rigorous treatment of errors have led to smaller lifetime errors and to lifetime values for the higher lying members of the various bands. We note the rather long sidefeeding times $\tau_{\rm SF}$ which, on average, are about twice as long as the level lifetimes. In agreement with an empirical rule previously found to be valid in $A\approx 80$ and $A\approx 150$ rotational nuclei, the sidefeeding time of a state is of the same order as the effective lifetime of its next discrete feeder state.

IV. DISCUSSION

A. Bandhead configurations

The previous work on the ground and excited states of ^{77}Rb as well as the band structures of neighboring nuclei, taken with the large transitional quadrupole moments in all the bands (see Sec. IV B), reinforces the evidence of the importance of the $Z=N=38$ shell gap at the large prolate deformation $\beta_2=+0.4$. The most important conclusion from

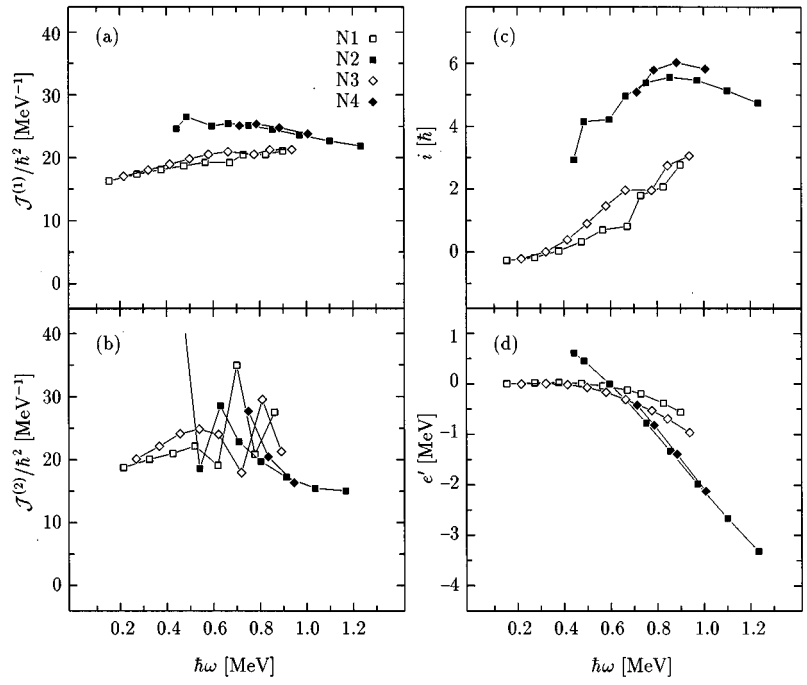

FIG. 11. Same as Fig. 10, but for the negative parity bands $N1-N4$.

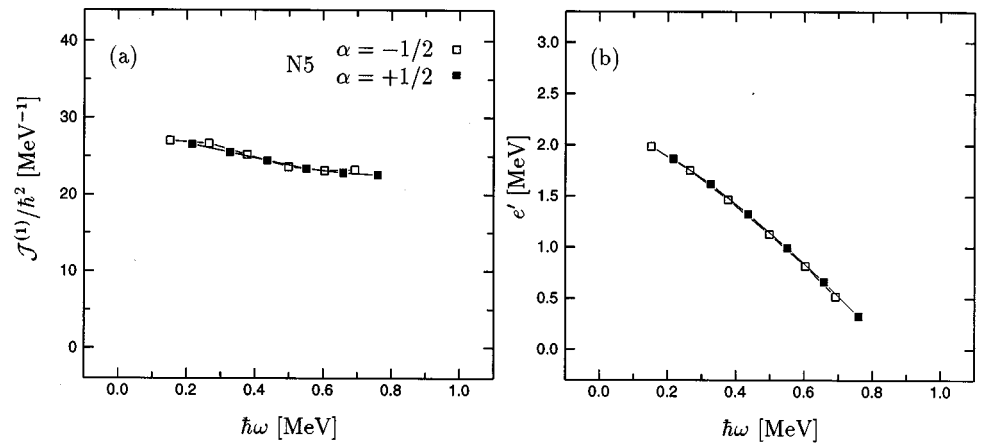

FIG. 12. Kinematical moment of inertia $\mathcal{J}^{(1)}/\hbar^2$ and aligned single-particle Routhian e' for the high-K band $N5$ in ^{77}Rb.

the previous studies is that this deformed shell gap is rather stable against both variations of the particle number and rotation. This implies that the arguments put forward in our recent studies on ^{76,78}Rb and ^{77}Sr [19,20] can also be taken as the starting point for assigning Nilsson orbits to the many bands in ^{77}Rb presented in Figs. 5–7. We would like to emphasize that the situation is very different if either the proton or neutron number starts deviating from 38 by more than two. In these nuclei (i.e., the light Se and Br nuclei [21] and the heavier Kr and Rb isotopes), strong polarization effects, coexistence of prolate and oblate states and complicated band crossing phenomena have been encountered.

The Nilsson diagram near the $N=Z=38$ deformed shell gap is shown in Fig. 8. It suggests that the structure of $^{77}_{37}\mathrm{Rb}_{40}$ should be governed by the $\pi[431\ 3/2^+]$ and $\pi[312\ 3/2^-]$ proton (hole) orbits and the $\nu[422\ 5/2^+]$, $\nu[303\ 5/2^-]$ and $\nu[301\ 3/2^-]$ neutron (particle) orbits. It is interesting to note that two positive and two negative parity orbits with similar K values, among them the low-K orbits of the $g_{9/2}$ proton and neutron spherical single-particle orbit, play an important role. The signature $\alpha=\pm 1/2$ ground bands of both parities ($P1/P2$ and $N1/N3$) have, indeed, been attributed to the $\pi[431\ 3/2^+] \otimes \nu^2[422\ 5/2^+]$ and $\pi[312\ 3/2^-] \otimes \nu^2[422\ 5/2^+]$ configurations which are predicted to be lowest in energy [6]. The crossing positive parity band $P3$ has recently been assigned a $\pi[431\ 3/2^+] \otimes \nu^2[301\ 3/2^-]$ configuration [6]. By similar arguments, the crossing negative parity bands $N2/N4$ could arise by either transferring the two neutrons into the $\nu[301\ 3/2^-]$ orbit or the two proton holes into the $\pi[310\ 1/2^-]$ orbit. The high-K negative parity band $N5$ is most likely built upon the mixed proton-neutron aligned configuration $\pi[431\ 3/2^+] \otimes \nu[422\ 5/2^+] \otimes \nu[301\ 3/2^-]$ (see below).

B. Quadrupole moments and moments of inertia

The $B(E2)$ values, moduli of the transitional quadrupole moments $|Q_t|$ and deformation parameters $|\beta_2|$, derived

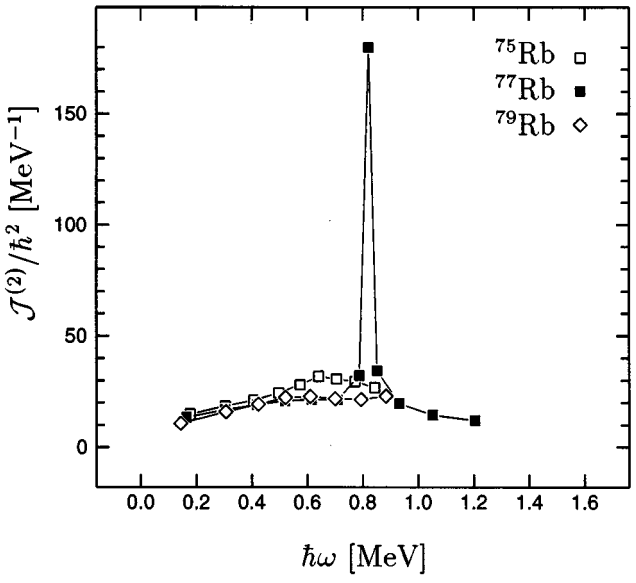

FIG. 13. Comparison of the dynamical moments of inertia, $\mathcal{J}^{(2)}/\hbar^2$, for the positive parity yrast bands in ^{75,77,79}Rb.

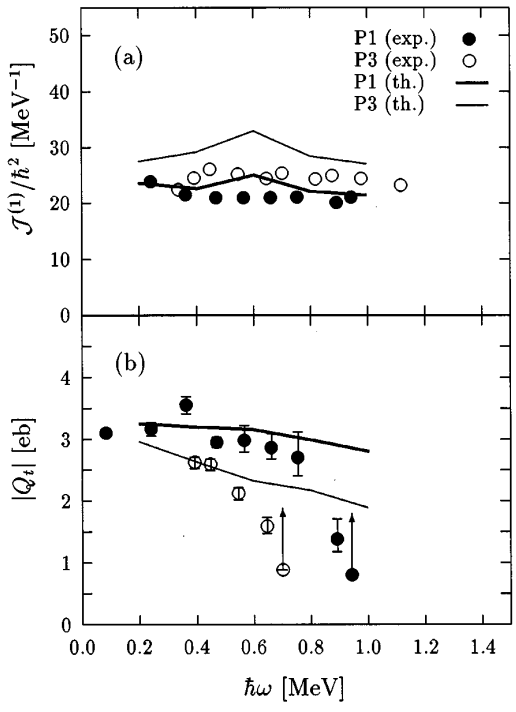

FIG. 14. Comparison of the values of $J^{(1)}$ and $|Q_t|$ in the $\pi = +$ bands with the results of the Nilsson-Strutinsky calculations by Dönau [6,22].

from the measured lifetimes and γ-ray energies and branching ratios, are listed in Table V. Taking somewhat arbitrarily the four lowest transitions in each band and using

$$Q_t = 3ZR_0^2\beta_2(1+0.16\beta_2)/\sqrt{5\pi} \quad (4)$$

(axial symmetry, $\gamma = 0$), we find the following deformations: $|\beta_2(P1)| = 0.38(1)$, $|\beta_2(P2)| = 0.35(2)$, $|\beta_2(P3)| = 0.28(2)$, $|\beta_2(N1/N2)| = |\beta_2(N3/N4)| = 0.42(2)$. These values confirm the previous finding of large deformations in all the bands, with those at negative parity being somewhat larger than those at positive parity [2]. A summary of all the measured transitional quadrupole moments $|Q_t|$ plotted versus the rotational energy $\hbar\omega$ is presented in Fig. 9, grouped according to parity. In the yrast bands $P1/P2$, $|Q_t| = 3.0e$ b essentially stays constant up to $\hbar\omega = 0.7$ MeV, while in the yrare band $P3$ the quadrupole moment is somewhat smaller at low $\hbar\omega$ and drops faster for increasing $\hbar\omega$. Harder *et al.* [6] have, indeed, correlated this difference in $|Q_t|$ between $P1/P2$ and $P3$ to the smaller prolate deformation of the $\nu[301\ 3/2^-]$ orbit relative to that of the $\nu[422\ 5/2^+]$ orbit. In the negative parity bands, $|Q_t|$ starts around 3.6 e b and steadily drops to about 2.0 e b at $\hbar\omega = 0.6$ MeV.

In the following, we will briefly discuss the frequency dependence of the kinematical and dynamical moments of inertia, $J^{(1)}/\hbar^2$ and $J^{(2)}/\hbar^2$, of the aligned spin i and of the single-particle Routhian, $e'(\omega)$. Again, we discuss the bands $P1$-$P3$ (Fig. 10), $N1$-$N4$ (Fig. 11) and $N5$ (Fig. 12) separately. As the various bands have been observed through their crossing points, the variations of the moments of inertia and the aligned spins can be determined accurately. We first note that in all the bands the kinematical moment of inertia is roughly constant with respect to rotational frequency and close to the rigid-rotor values $J_{\rm rig}/\hbar^2 = 21\ {\rm MeV}^{-1}$, evaluated for the prolate deformation $\beta_2 = +0.4$ and the nuclear radius $R_0 = 1.2A^{1/3}$ fm. Another general observation refers to the relative change of the kinematical moments of inertia of the crossing bands ($P3$, $N2/N4$) relative to those in the ground bands ($P1/P2$, $N1/N3$): The crossing bands $P3$, $N2$, and $N4$ clearly have larger $J^{(1)}$ values. It is also interesting to note that the $J^{(1)}$ values of the excited bands $P3$, $N2$, $N4$, and $N5$ nearly overlap with each other at any given rotational frequency and all of them show a slight tendency to decrease for increasing $\hbar\omega$. In spite of the very smooth behavior of the kinematical moments of inertia in all the

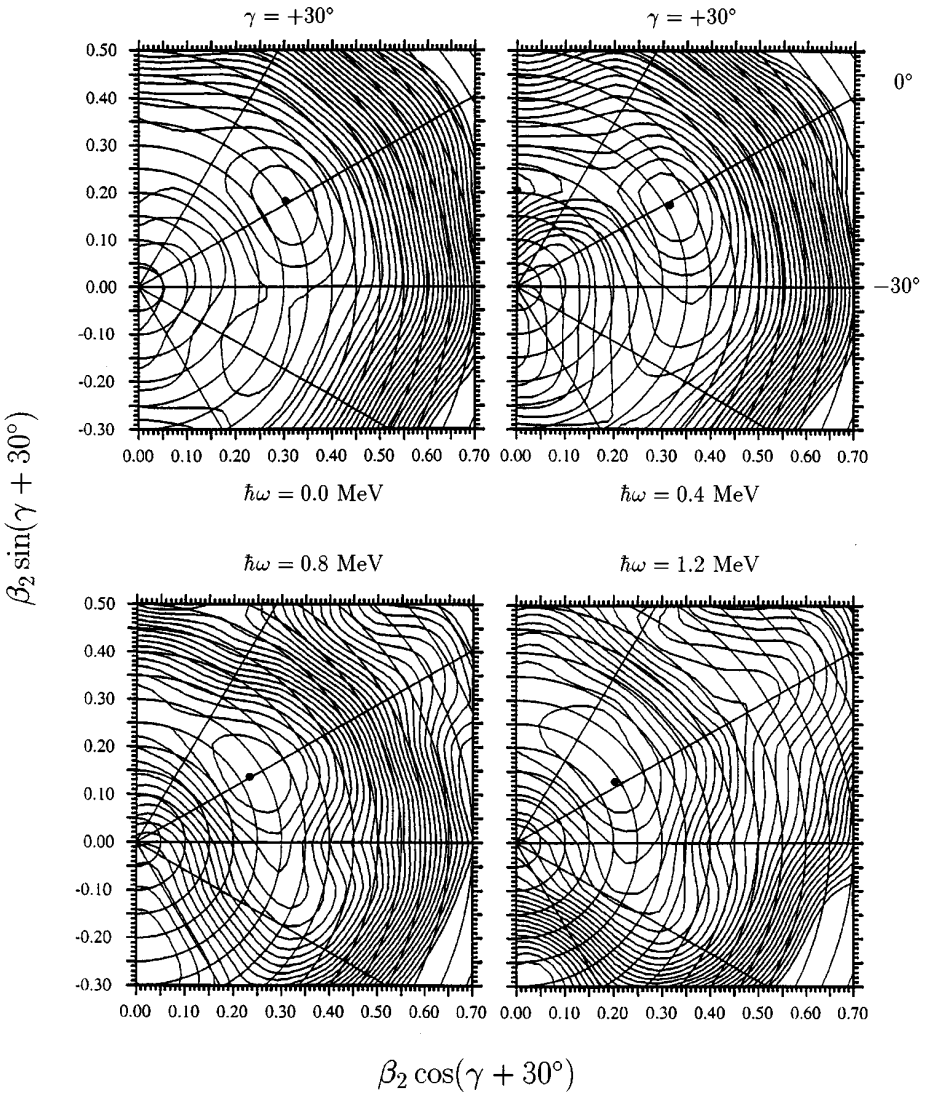

FIG. 15. Calculated total Routhian surface for the $\pi = +$ band $P1$ [23]. Note the very stable minimum at axially symmetric prolate deformation.

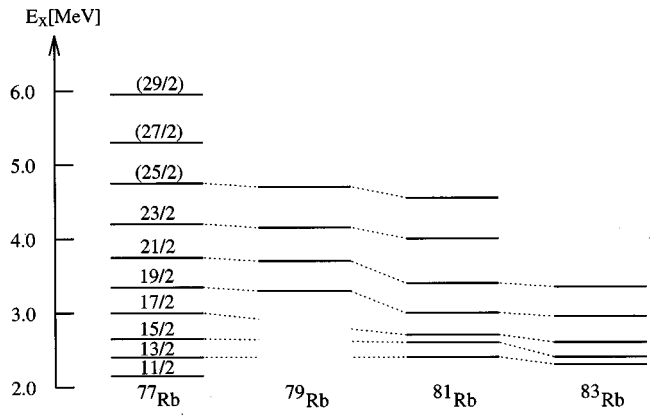

FIG. 16. The members of the presumed high-K bands in the odd-A Rb isotopes $^{77-83}$Rb.

bands, the dynamical moments $J^{(2)}$ show appreciable local fluctuations but, apart from these, average again at the rigid-body value.

C. Cranked shell model calculations

The unusual crossing of the favored yrast and yrare $\pi=+$ bands $P1/P3$ in ^{77}Rb was recently explained in our earlier publication [6]. Without repeating the detailed reasoning given there, we present here the main results. This crossing is *not* a consequence of the common s-band mechanism where two identical particles in high-j orbits align their spins, but is associated with the two different $(3qp)$ configurations mentioned in Sec. IV A. With respect to the $N=Z=38$ shell closure at $\beta_2=+0.4$, these configurations are $\pi[431\ 3/2^+]\otimes\nu^2[422\ 5/2^+]$ in band $P1$ and $\pi[431\ 3/2^+]\otimes\nu^2[301\ 3/2^-]$ in band $P3$. This interpretation is supported by the neighboring odd-A isotopes ^{75}Rb and ^{79}Rb which have one neutron pair less (more) than ^{77}Rb and which, for this reason, do not show the same type of band crossing as $P1/P3$ in ^{77}Rb. Figure 13 illustrates this, showing the evolution of the dynamic moment of inertia, $J^{(2)}/\hbar^2$, along the $\pi=+$ yrast states $P1/P3$ in these three isotopes: While the pronounced ''band crossing'' occurs in ^{77}Rb at $\hbar\omega\approx 0.7$ MeV, $J^{(2)}$ stays nearly constant in ^{75}Rb and ^{79}Rb, where the $\nu[522\ 5/2^+]$ and $\nu[301\ 3/2^-]$ orbits are either both empty or both filled.

Nilsson-Strutinsky-type calculations, without any static pairing correlations included, have been carried out by Dönau [6,22]. The resulting moments of inertia $J^{(1)}$ and quadrupole moments $|Q_t|$ are inserted in Fig. 14. The calculations reproduce the measured values rather well, in particular the near-constant $J^{(1)}$ values and the slowly decreasing quadrupole moments. The calculations also account for the observations, concerning the relative magnitude of the mass and quadrupole moments, i.e., $J^{(1)}(P1)<J^{(1)}(P3)$ and $|Q_t(P1)|>|Q_t(P3)|$.

Cranked shell model calculations with a deformed Woods-Saxon potential and reduced pairing gap have been performed by Wyss [23]. The resulting total Routhian surfaces for the positive parity ground band $P1$ at $\hbar\omega=0$, 0.4, 0.8, and 1.2 MeV are shown in Fig. 15. One notes the very stable prolate minimum ($\gamma=0°$) at $\beta_2=0.35$ for $\hbar\omega=0$ MeV which develops to $\beta_2=0.25$ above $\hbar\omega=0.8$ MeV.

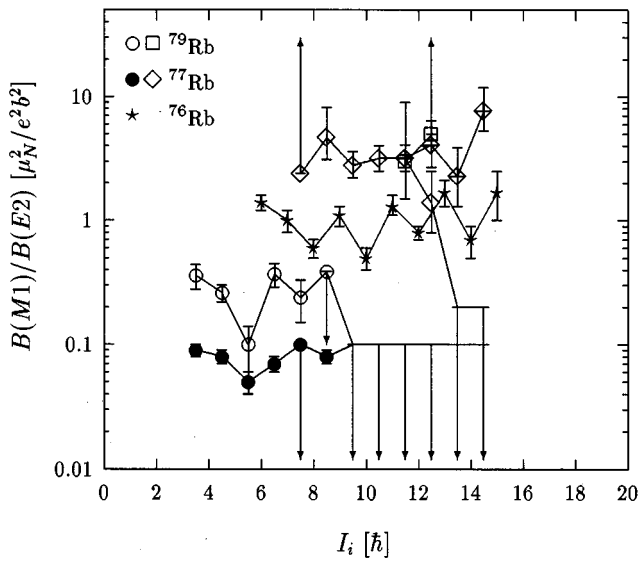

FIG. 17. Ratios $R_{12}=B(M1)/B(E2)$ for the bands $N1$, $N3$, $N5$ in ^{77}Rb and ^{79}Rb and the aligned proton-neutron band in ^{76}Rb.

Similar calculations have also been carried out by Sheikh [24] for the $P1$ and $N1$ bands. The predicted deformations of the positive and negative parity ground bands are $+0.37$ and $+0.39$ to be compared with $\beta_2=0.38(1)$ and $\beta_2=0.42(2)$. The energy difference of the two band heads is 120 keV.

D. The high-K band

In the discussion of Fig. 12, we have already pointed out the near constancy of the $J^{(1)}$ values in this band and have tentatively given its configuration, involving a rotational-aligned $[431\ 3/2^+]$ proton and $[422\ 5/2^+]$ neutron, besides a $[301\ 3/2^-]$ neutron. Few members of bands with similar origin have been found [25–27] in the heavier odd-A Rb isotopes ^{79,81,83}Rb (see Fig. 16) and have also been extensively studied in ^{83}Y [28–30]. The Nilsson-Strutinsky calculations by Sheikh [24] predict that the lowest two $K^\pi=11/2^-$ bandheads have $E_x\simeq 2.0$ MeV ($\beta_2=0.39$) and $E_x\simeq 2.8$ MeV ($\beta_2=0.35$). Their configurations are either $\pi[422\ 5/2^+]\otimes\pi[431\ 3/2^+]\otimes\pi[312\ 3/2^-]$, i.e., a proton excitation across the Z=38 gap, or $\pi[431\ 3/2^+\otimes\nu[422\ 5/2^+]\otimes\nu[312\ 3/2^-]$. The very different nature of this band $N5$ can also be seen in the ratio $R_{12}=B(M1)/B(E2)$ of $M1$ and $E2$ decay strengths deduced from the experimental $\Delta I=-1$ and $\Delta I=-2$ branching ratios. In Fig. 17, this ratio (or its limit whenever only one branch has been identified) is plotted as a function of the spin for the negative parity bands in ^{77}Rb and ^{79}Rb and the aligned $K^\pi=4^-$ proton-neutron band in ^{76}Rb we have recently identified [19]. The data clearly fall into three classes: the low-K ground bands in ^{77,79}Rb have $R_{12}<0.5$, while the high-K bands in ^{77,79}Rb average at $R_{12}>2$. In spite of a regular odd-even spin staggering of the R_{12} values in the proton-neutron band in ^{76}Rb, the average ratio there is $R_{12}\approx 1$.

V. CONCLUSIONS

The present detailed work on the band structures of ^{77}Rb has increased the knowledge of this very deformed

nucleus considerably. Besides extending the known rotational bands to much higher spins, we have identified several new bands. The very good statistics has allowed us to determine many state lifetimes and sidefeeding times from the Doppler broadened line shapes. This has resulted in precise deformation parameters in nearly all the bands as a function of the rotational frequency. We note, however, that lifetime measurements in the band $N5$ are urgently needed.

The role of the $N=Z=38$ single-particle gap at $\beta_2 = +0.4$ has been decisive in understanding experimental features such as the near-rigid rotational behavior in the bands, the unusual crossing of the $\pi = +$ yrast and yrare bands $P1/P3$ and the structure of the proton-neutron aligned band $N5$. The completeness of the ^{77}Rb level scheme now achieved as well as the rich material recently gathered for the neighboring light Rb and Kr isotopes calls for a comprehensive theoretical approach to these nuclei.

ACKNOWLEDGMENTS

The authors wish to thank R. Darlington for the preparation of the ^{40}Ca targets and C. Baktash, R. Bark, J. D. Garrett, F. Hannachi, D. Sarantites and the crew and staff of the NSF and the NBITAL for their assistance in the experiments. We are most grateful to F. Dönau, J. A. Sheikh, and R. Wyss for their advice on the interpretation of the band structures and the permission to quote from their calculations. This work was funded in part by Deutsches Bundesministerium für Bildung, Wissenschaft, Forschung und Technologie (BMBF) under Contract No. 06GÖ677, the Swedish Natural Science Research Council, the Danish Natural Science Research Council, and the U.S. Department of Energy under Contract Nos. DE-AC05-76OR00033 and DE-AC05-84OR-21400. EUROGAM was funded by the U.K. Science and Engineering Research council and IN2P3, France.

[1] C. J. Lister *et al.*, Phys. Rev. C **28**, 2127 (1983).
[2] L. Lühmann *et al.*, Europhys. Lett. **1**, 623 (1986).
[3] W. Nazarewicz *et al.*, Nucl. Phys. **A435**, 397 (1985).
[4] W. Nazarewicz and T. Werner, in *Nuclear Structure of the Zirconium Region*, edited by R. A. Meyer, J. Eberth and K. Sistemich (Springer, Berlin, 1988), p. 277.
[5] C. Thibault *et al.*, Phys. Rev. C **23**, 2720 (1981).
[6] A. Harder *et al.*, Phys. Lett. B **374**, 277 (1996).
[7] C. W. Beausang and J. Simpson, J. Phys. G **22**, 527 (1996); P. J. Nolan, F. A. Beck, and D. B. Fossan, Annu. Rev. Nucl. Part. Sci. **45**, 561 (1994).
[8] C. W. Beausang *et al.*, Nucl. Instrum. Methods Phys. Res. A **313**, 37 (1992).
[9] A. N. James *et al.*, Nucl. Instrum. Methods Phys. Res. **212**, 545 (1983).
[10] A. N. James *et al.*, Nucl. Instrum. Methods Phys. Res. A **267**, 144 (1988).
[11] M. K. Kabadiyski, K. P. Lieb, and D. Rudolph, Nucl. Phys. **A563**, 301 (1993).
[12] S. E. Arnell *et al.*, Nucl. Instrum. Methods Phys. Res. A **300**, 303 (1991).
[13] T. Kuroyanagi *et al.*, Nucl. Instrum. Methods Phys. Res. A **316**, 289 (1992).
[14] G. Winter, Nucl. Instrum. Methods Phys. Res. **214**, 537 (1983).
[15] G. Winter, program DOPPIDIF, Rossendorf (1983).
[16] J. Lindhard, V. Nielsen, and M. Scharf, Mat. Fys. Medd. K. Dan. Vidensk. Selsk. **36**, no. 10 (1968).
[17] F. Cristancho and K. P. Lieb, Nucl. Phys. **A480**, 353 (1988).
[18] L. Lühmann, Ph. dissertation, Universität Göttingen, 1985, unpublished.
[19] A. Harder *et al.*, Phys. Rev. C **51**, 2932 (1995).
[20] C. J. Gross *et al.*, Phys. Rev. C **49**, R580 (1994).
[21] K. P. Lieb, L. Lühmann, and B. Wörmann, in *Nuclei Off the Line of Stability*, edited by R. A. Meyer and D. Brenner (Am. Chem. Soc., Washington, 1986), p. 233.
[22] F. Dönau, private communication.
[23] R. Wyss, private communication.
[24] J. A. Sheikh, private communication.
[25] J. W. Holcomb *et al.*, Phys. Rev. C **48**, 1020 (1993).
[26] J. Döring *et al.*, Phys. Rev. C **50**, 1845 (1994).
[27] W. Gast *et al.*, Phys. Rev. C **22**, 469 (1980).
[28] K. Bharuth-Ram *et al.*, Phys. Lett. B **252**, 540 (1990).
[29] F. Cristancho *et al.*, Nucl. Phys. **A540**, 307 (1992).
[30] T. D. Johnson *et al.*, Z. Phys. A **347**, 285 (1994).